Coupling between surface plasmons in subwavelength hole arrays

Jean-Baptiste Masson and Guilhem Gallot*

Laboratoire d'Optique et Biosciences, Ecole Polytechnique - CNRS UMR 7645 - INSERM U696, 91128 Palaiseau, France
(Received 23 January 2006; published 13 March 2006)

The coupling between the surface plasmons of two overlapping arrays of orthogonally oriented subwavelength elliptical holes has been demonstrated by terahertz time-domain spectroscopy over the 0.1–1 THz range. This enhanced transmission exhibits polarization sensitive frequency shift. Three-dimensional numerical simulations provide precise insight in the energy redistribution of the surface plasmons through the subwavelength holes. A simple theoretical model, demonstrating a strong coupling between the two subarrays, exhibits good agreement with the experimental data.

In the recent years, the demonstration of a strong and unexpected enhancement of light transmission through arrays of subwavelength holes[1] has generated numerous experimental and theoretical works. Enhancement of several order of magnitudes has been reported,[2] with respect to standard aperture theory.[3,4] The transmission can even exceed the surface ratio occupied by the holes, implying that light is focused by the structure of the arrays through the holes. This extraordinary transmission is generally admitted to be due to excitation of surface plasmons (SPs) on the upper and lower surfaces of the metallic array.[5–7] These results are stimulating in numerous fields:[8–11] Near-field microscopy, high-density storage, detection of molecules of chemical and biological interest, photolithography, and light-emitting diodes (LEDs). Since this discovery, many experiments have been performed to characterize and modelize this abnormal transmission, in the optical,[7,8,12–19] infrared,[20,21] and terahertz ranges.[5,22–25] These studies involved the influence of shape and hole diameter,[6,14,26,27] lattice geometry,[1] or film thickness,[15] but so far only arrays of identical holes have been investigated, and the true influence of the shape of the holes on the SP generation still remained sketchy, in particular on the frequency shifts associated with.

In this letter, we demonstrate, experimentally and theoretically, enhanced transmission with polarization sensitive frequency shifts, which arises from the coupling between SPs modes from two overlapping arrays of orthogonally oriented subwavelength elliptical holes. Furthermore, we establish the complex link between the shape of the holes and the properties of the surface plasmons, in particular its frequency resonance, and this leads to the validation of the Fano model for SPs. The array is made of a free-standing thin metal plate. The enhanced transmission of the array is measured by terahertz time-domain spectroscopy (THz-TDS).[28] Broadband linearly polarized subpicosecond single cycle pulses of terahertz radiation are generated and coherently detected by illuminating photoconductive antennas with two synchronized femtosecond laser pulses. Rotation of the sample with respect to the linear incident polarization allows us to investigate the nature of the coupling between the SPs. Numerical Fourier transform of the time-domain signal gives access to the characteristic transmission spectrum of the array.

The sample is a free-standing 18-μm-nickel-plate array of subwavelength elliptical holes, fabricated by electroforming.

The array has a $L=600$ μm period, with 400×200 μm ellipses, whose long axis are alternatively aligned along the x and y directions (inset of Fig. 1). The total array is then made of two ellipse subarrays, one with the ellipse long axis along x (x-ellipse) and the other along y (y-ellipse). The total array is then anisotropic, the periodicity is 1200 μm along x and 600 μm along y. The precision for the hole dimensions and periodicity is better than 1 μm. The aperture ratio to the total plate area is about one-sixth, equivalent to the geometric transmission. The sample is positioned on a 10-mm-circular aperture, in the linearly polarized, frequency independent, 4.8-mm-waist Gaussian THz beam ($1/e$ in amplitude). A precise rotation stage adjusts the angle θ between axis x of the array and the linear THz polarization. The dynamics of the surface plasmons is then recorded during 150 ps, yielding a 8-GHz-frequency precision after numerical Fourier transform. A reference scan is taken with empty aperture.

The transmission of the metal array is calculated by the amplitude ratio of the complex spectra of the metal plate and reference scan for several polarization orientations, as given in Fig. 1. For each orientation, we observe a strongly enhanced resonance peak between 0.4 and 0.5 THz, followed at higher frequency by a much broader continuumlike area.
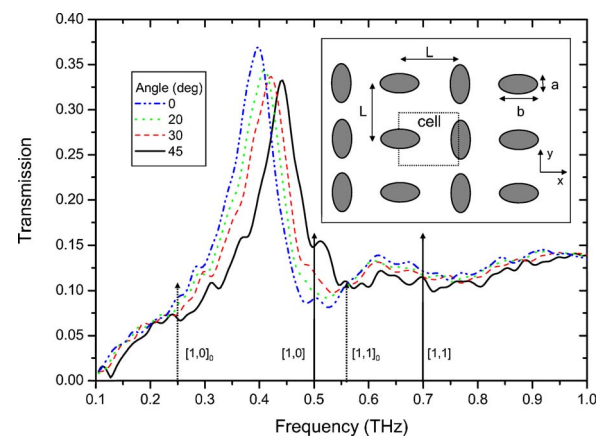

FIG. 1. (Color online) Experimental amplitude transmission, for incident linear polarization at 0, 20, 30, and 45°. The vertical arrows show the position of the integer modes of the total array $[i,j]$ and the subarrays $[i,j]_0$. The inset depicts the periodic structure of the ellipses. $L=600$ μm, $a=200$ μm, $b=400$ μm.
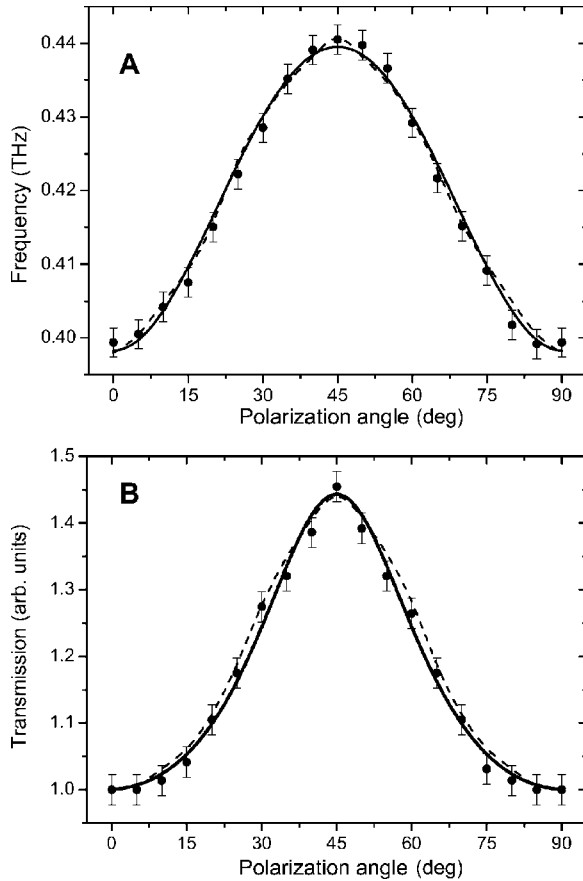
FIG. 2. Resonance frequency shift (A) and amplitude transmission at 0.5 THz (B) versus incident polarization angle. Experimental data (dots) are compared to numerical simulations (dashed line) and theoretical model (solid line). For the model, $A=0.117$ THz and $B=0.15$ THz.

The amplitude enhancement, compared to the geometrical transmission is 2 (4 in power transmission). We also notice a strong shift of the resonance frequency with respect to the incident polarization, as shown in Fig. 2(A), contrary to previous work on identical ellipse arrays.[14] The resonance frequency is 0.40 THz for the linear polarization along the x axis, and 0.44 THz at 45°, corresponding to a 10% relative shift. This shift is symmetric with respect to 45° within experimental precision. Furthermore, none of the resonance frequencies coincides with the integral orders of SP modes $\nu(i,j)=\frac{c}{L}\sqrt{i^2+j^2}$,[1] where i and j are integers, as depicted by the vertical solid arrows in Fig. 1. Likewise, these new frequencies cannot originate in one of the subarrays, whose resonance frequencies are given by $\nu(i,j)_0=\frac{c}{2L}\sqrt{4i^2+j^2}$ (vertical dashed arrows in Fig. 1). The normalized amplitude variations at 0.5 THz [Fig. 2(B)] also exhibit the same symmetry. This frequency has been chosen as the first resonant mode from integral order theory [1,0]. The amplitude is normalized, so that the transmission is 1 at $\theta=0°$.

To get a better picture of these new resonances, we have performed numerical simulations. We carried out a direct resolution of Maxwell's equations through a full three-dimensional (3D) ab initio finite element method (FEM) analysis of the electric field propagating through the array.[29]

This method provides quantitative information on the SP distribution in the metal array. It allows the calculation of the transmitted THz electromagnetic field and takes into account the near-field effects on the array. To reduce the size of the simulation box, we used a unitary cell of two halves of the ellipses (see inset of Fig. 1), with adequate symmetry conditions. The complex electromagnetic fields have been calculated in two sets of simulations, for an incident plane wave of linear polarization in the x and y directions, namely $\mathbf{E_x}$ and $\mathbf{E_y}$. This allows the calculation of the fields for any orientation of the polarization by $\mathbf{E}(\theta)=\mathbf{E_x}\cos(\theta)+\mathbf{E_y}\sin(\theta)$. The precision of the simulations are controlled by progressively reducing the adaptive mesh size, in particular in the elliptical holes. Typical mesh dimensions are $\lambda/700$ in the holes and $\lambda/5$ outside, yielding precision better than 0.5%. The relative permittivity of nickel is $\epsilon=-9.7\times10^3+1.1\times10^5i$, and relative permeability is 100.[30,31]

We calculated the electric field density at 0.44 THz, on the output hole and metal surface of the array, using the same dimensions as in the experiment, for three incident polarization orientations: $\theta=45°$ [Fig. 3(A)], 30° [Fig. 3(B)], and 60° [Fig. 3(C)]. The field density is characteristic of the SP at the surface of the metal. A strong anisotropy of the density can be observed, correlated with high-field density in the elliptical holes and in particular on the edges. The field concentration on the ellipse edges goes far below the wavelength, typically $\lambda/50$, which is characteristic of near-field interactions. We also notice a complex pattern at the surface of the metal. These density-line loops are highly evocative of the SPs on metal.[7] For $\theta=45°$, the energy density is approximately equally distributed between the x and y ellipse [Fig. 3(A)]. It is slightly higher in the x ellipse due to the structure anisotropy of the total array. A dramatic change in the density distribution occurs when the incident polarization is changed to $\theta=30°$ or $\theta=60°$. The energy shifts toward the x ellipse at 30°, whereas it shifts toward the opposite direction (y ellipse) at 60°. The energy localization is then strongly controlled by the incident polarization direction. The resonant density-line loops are also affected, showing that the coupling between the x and y ellipse is modulated by the polarization. It should also be noted that more energy exits from the holes with polarization at 45° than at 30° or 60°, in agreement with data at 0.44 THz, suggesting a better coupling between the ellipses at 45°. To further study the coupling between the two subarrays, we computed the field pattern of each subarray independently. The difference between the field density of the total array and the sum of the field densities of both subarrays individually, at $\theta=45°$ is shown in Fig. 3(D). The difference clearly demonstrates that the total field distribution in the metal array cannot be described by the linear superposition of the two subarray contributions, and then implies polarization-dependent coupling between the subarrays. We calculated the transmission spectra from these 3D simulations. Results are depicted in Fig. 4. The computed spectra reproduce well the polarization-dependent behavior observed in the experiment, as well as the asymmetric Fano-type profiles. We also extracted from the computed spectra the resonance displacement and amplitude variations. The results [dashed lines in Figs. 2(A) and 2(B)] are in very good agreement with the experimental data, which validates the simulations.
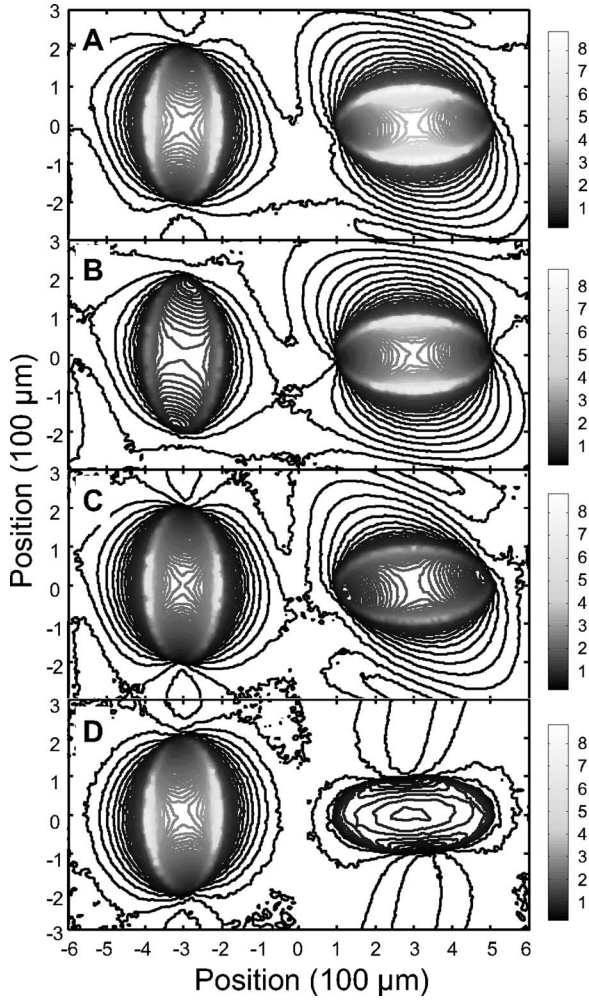
FIG. 3. (A)–(C) Numerical simulations of the total time-averaged $|E|$ electric field at the surface of the array. Incident polarizations are 45°(A), 30°(B), and 60°(C) and frequency is 0.44 THz. (D) Difference between the field density of the total array and the sum of the densities for each subarray, at 45°. The gray scale is the same in all the pictures.

A simple picture of the coupling between the two subarrays can be obtained considering the superimposition of the two orthogonally-oriented ellipse subarrays. The abnormal transmission of each subarray is given by a Fano-type model,[32] which can be used to model the enhanced resonance profiles through subwavelength hole arrays.[33] It describes the coupling between a continuum of states $|k\rangle$ from the scattering of the incident plane wave by the geometrical holes, and a resonant state $|a\rangle$ from discrete resonant SP excitations of the illuminated interface of the array [see Fig. 5(A)]. The level of each subarray is given by the integral order mode, namely $\nu(1,0)_0 = \nu_0 = 0.25$ THz. This means that each subarray exhibits a resonance frequency at 0.25 THz, and a Fano profile from the coupling with the continuum. The total array is the superimposition of the two subarrays, and is then described by the coupling of two degenerate levels $|a\rangle$ and $|b\rangle$ at 0.25 THz [see Fig. 5(B)]. When the two subarrays are identical, the matching is perfect and the result is equivalent to an array with half the initial period and then a resonance
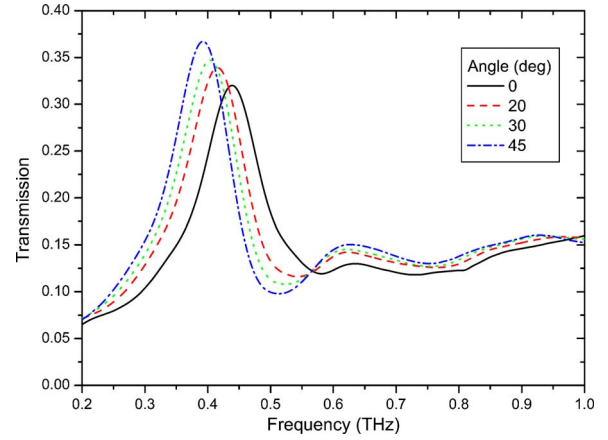

FIG. 4. (Color online) Transmission amplitude spectra computed by three-dimensional finite element methods numerical simulations, for four incident polarization angles. Simulation parameters match the ones of the experiment.

frequency $2\nu_0$. The coupling can be a direct interaction between $|a\rangle$ and $|b\rangle$, or it may involve an intermediate coupling with the continuum $|k\rangle$. The resulting Hamiltonian of these first- and second-order interactions is then given by the following matrix elements,[34] respectively,

$$\langle b|W|a\rangle = hA \sin 2\theta \tag{1}$$

and

$$\sum_{k \neq a,b} \frac{\langle b|W|k\rangle\langle k|W|a\rangle}{E_0 - E_k} = ihB, \tag{2}$$

where W is the coupling term, A and B are constants and $E_0 = h\nu_0$. The direct coupling between $|a\rangle$ and $|b\rangle$ is polarization sensitive because each subarray, due the its specific orientation, exhibits strong preferential polarization transmission.[14] The polarization sensitive $\sin 2\theta$ coupling originates in the geometrical symmetries of the total array and is confirmed by the numerical simulation, where it is maximum at 45°. The complex value of the indirect interaction comes from the $\pi/2$ dephasing between the transition amplitudes of the first- and second-order interactions. The Hamiltonian of the interaction is then
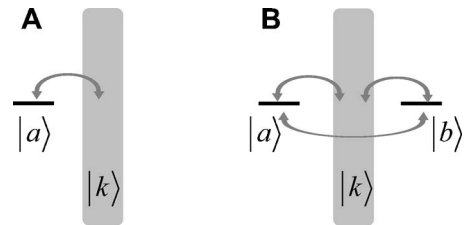

FIG. 5. (A) Fano model of a subwavelength hole array and the coupling between a continuum of states $|k\rangle$ and a resonant level $|a\rangle$. (B). Extension to the coupling between two subarrays of resonant levels $|a\rangle$ and $|b\rangle$.

$$H = h \begin{pmatrix} \nu_0 & 0 \\ 0 & \nu_0 \end{pmatrix} + h \begin{pmatrix} 0 & A \sin 2\theta + iB \\ A \sin 2\theta - iB & 0 \end{pmatrix}. \tag{3}$$

The total array is then similar to degenerate levels at 0.25 THz linked together by a polarization sensitive coupling. The eigenvalues of the Hamiltonian are

$$\nu_{\pm} = \nu_0 \pm \sqrt{\tfrac{1}{2} A^2 (1 - \cos 4\theta) + B^2}. \tag{4}$$

Therefore, the coupling removes the degeneracy at 0.25 THz, predicting new frequencies, one redshifted (ν_-), the other blueshifted (ν_+). The blueshifted new level is easily assimilated to the observed enhanced resonance peak. The fit of the frequency shift [solid line in Fig. 2(A)] is excellent with $A = 0.117$ THz and $B = 0.15$ THz. The other level ν_- lies below 0.1 THz. Therefore, the scattering efficiency is very weak and its influence can be neglected. We can define a matching efficiency $\rho = (\nu_+ - \nu_0)/\nu_0$, equal to 1 for a perfect matching and 0 for independent arrays. Here, the matching efficiency ranges from 60% at $\theta = 0°$ and 90°, to 76% at $\theta = 45°$, showing a preferential shape matching of the orthogonal ellipses with the incident polarization at 45°. Furthermore, the amplitude modulation at 0.5 THz was calculated with the same coupling coefficient, with a Fano profile[32] for the resonance. The Fano profile parameters have been adjusted with the 45° data, and remain constant for the other frequencies. Once again, the agreement between this model and the experimental data is very good [Fig. 2(B)]. The polarization mediated strong coupling between the two subarrays allows the redistribution of the energy in holes, and then favors the light transmission through the holes.

Comparison with Bloch wave analysis can be discussed here. Even though polarization dependence has been observed in elliptical arrays,[35] a simple model approach with symmetry consideration of Bloch waves would encounter major difficulties in our case. Indeed, this approach leads to linear amplitude superposition of Bloch modes, with no polarization global frequency shifts. Furthermore, a simple Bloch waves analysis does not reveal the whole complexity of the influence of the shape of the holes, as discussed in many papers.[14,36,37] Although a complex modelization, by the exact treatment of the symmetry properties of the lattice basis could probably be considered using Wanier functions formalism,[38] we can understand the observed data with a simple model.

In conclusion, we studied, experimentally and theoretically, the enhanced transmission from the overlapping of two subwavelength subarrays in the 0.1–1 THz range with 8 GHz resolution. The transmission spectra exhibits strong polarization sensitive frequency resonance shifts, at frequencies that are not predicted by the classical integer modes theory, and is an important result in favor of the Fano model for surface plasmons. This shift is found to be due to the strong coupling between the two subarrays, and has promising applications in tunable devices. Furthermore, numerical simulations point out the control of the energy distribution by the incident polarization, that will extend the potential of these subwavelength structures.

*Corresponding author. Email address: guilhem.gallot @polytechnique.fr

[1] T. W. Ebbesen *et al.*, Nature (London) **391**, 667 (1998).
[2] A. Nahata *et al.*, Opt. Lett. **28**, 423 (2003).
[3] H. A. Bethe, Phys. Rev. **66**, 163 (1944).
[4] C. J. Bouwkamp, Rep. Prog. Phys. **17**, 35 (1954).
[5] J. Gomez Rivas *et al.*, Phys. Rev. B **68**, 201306(R) (2003).
[6] D. Qu *et al.*, Opt. Lett. **29**, 896 (2004).
[7] W. L. Barnes *et al.*, Nature (London) **424**, 824 (2003).
[8] T. J. Kim *et al.*, Opt. Lett. **24**, 256 (1999).
[9] Y. Liu and S. Blair, Opt. Lett. **28**, 507 (2003).
[10] R. Sambles, Nature (London) **391**, 641 (1998).
[11] J. Vuckovic *et al.*, IEEE J. Quantum Electron. **36**, 1131 (2000).
[12] L. Martin-Moreno *et al.*, Phys. Rev. Lett. **86**, 1114 (2001).
[13] S. C. Hohng *et al.*, Appl. Phys. Lett. **81**, 3239 (2002).
[14] R. Gordon *et al.*, Phys. Rev. Lett. **92**, 037401 (2004).
[15] A. Degiron *et al.*, Appl. Phys. Lett. **81**, 4327 (2002).
[16] E. Altewischer *et al.*, Nature (London) **418**, 304 (2002).
[17] E. Devaux *et al.*, Appl. Phys. Lett. **83**, 4936 (2003).
[18] W. L. Barnes *et al.*, Phys. Rev. Lett. **92**, 107401 (2004).
[19] A. Dogariu *et al.*, Appl. Phys. B: Lasers Opt. **74**, S69 (2002).
[20] Q. Cao and P. Lalanne, Phys. Rev. Lett. **88**, 057403 (2002).

[21] Y.-H. Ye and J.-Y. Zhang, Appl. Phys. Lett. **84**, 2977 (2004).
[22] D. Qu and D. Grischkowsky, Phys. Rev. Lett. **93**, 196804 (2004).
[23] F. Miyamaru and M. Hangyo, Appl. Phys. Lett. **84**, 2742 (2004).
[24] J. G. Rivas *et al.*, Opt. Express **13**, 847 (2005).
[25] H. Cao and A. Nahata, Opt. Express **12**, 1004 (2004).
[26] T. Thio *et al.*, J. Opt. Soc. Am. B **16**, 1743 (1999).
[27] A. K. Azad *et al.*, Appl. Phys. Lett. **86**, 141102 (2005).
[28] D. Grischkowsky *et al.*, J. Opt. Soc. Am. B **7**, 2006 (1990).
[29] Femlab, Comsol Inc., Burlington, MA.
[30] M. A. Ordal *et al.*, Appl. Opt. **22**, 1099 (1983).
[31] *Magnetic Properties of Metals*, Landolt-Bornstein, Group III: Condensed Matter (Springer-Verlag, Berlin, 1986).
[32] U. Fano, Phys. Rev. **124**, 1866 (1961).
[33] C. Genet *et al.*, Opt. Commun. **225**, 331 (2003).
[34] C. Cohen-Tannoudji *et al.*, *Atom-Photon Interactions: Basic Processes and Applications* (Wiley-Interscience, New York, 1998).
[35] J. Elliott *et al.*, Phys. Rev. B **70**, 233403 (2004).
[36] Q.-J. Wang *et al.*, Appl. Phys. Lett. **87**, 091105 (2005).
[37] K. J. Klein Koerkamp *et al.*, Phys. Rev. Lett. **92**, 183901 (2004).
[38] C. Kittel, *Introduction to Solid State Physics* (Wiley, Chichester, 1996).